Acoustic power transfer for biomedical implants using piezoelectric receivers: effects of misalignment and misorientation

Hamid Basaeri¹, Yuechuan Yu², Darrin Young² and Shad Roundy¹

- Department of Mechanical Engineering, University of Utah, Salt Lake City, UT, United States of America
- ² Department of Electrical and Computer Engineering, University of Utah, Salt Lake City, UT, United States of America

E-mail: h.basaeri@utah.edu

Received 29 March 2019, revised 17 May 2019 Accepted for publication 29 May 2019 Published 13 June 2019



Abstract

Implantable medical devices (IMDs) can be powered wirelessly using acoustics with no need for a battery. In an acoustic power transfer system, which consists of a transmitter, medium, and a receiver, the power that the receiver generates is a function of its position (depth, orientation, and alignment relative to the transmitter). The power delivered to the implant should remain stable and reliable even with possible uncertainties in the location of the implant. In this paper, we compare two common designs for piezoelectric ultrasonic transducers that can be used for acoustically powering IMDs, and study their generated power sensitivity to any change in their location. Although commercial off-the-shelf (COTS) transducers are widely being used in the literature, they may not be the best candidate for powering small implants since they may not be able to provide sufficient power in the presence of location uncertainties. Piezoelectric micromachined ultrasonic transducers (pMUTs) are diaphragm structures and are also suitable for wirelessly powering implants. We present a pMUT receiver and study the sensitivity of the generated power of the pMUT to changes in its position. We then perform a comparative study between power generation capability of our pMUT and a COTS transducer with the same lateral dimensions as the pMUT. We observed that the generated power from a pMUT structure is less sensitive to misorientation and misalignment of the device. The average percentage improvement in the generated power from pMUT compared to COTS are 86%, 917%, and 111% for depth, alignment, and orientation, respectively.

Keywords: piezoelectric micromachined ultrasonic transducer, acoustics power transfer, bulk-mode transducer, ultrasonic generator

1

(Some figures may appear in colour only in the online journal)

1. Introduction

The use of implantable medical devices (IMDs) for monitoring human health is growing rapidly. These devices are usually designed to monitor biological parameters, deliver drugs, or improve the function of particular organs in the human body. IMDs require a sufficient and stable source of power in order to perform their tasks properly. The need for wirelessly powering IMDs is significantly increasing as batteries are not often the best candidate to power these devices due to their limited lifetime and large size [1]. The power required for IMDs is generally on the order of hundreds of microwatts to tens of milliwatts at the extreme high end [2, 3]. For example, pacemakers usually require a power below 100 μ W while cochlear implants need around 1 mW to 10 mW to operate [4]. Kinetic energy harvesting has been implemented

as a method to power implantable devices such as pacemakers [5, 6]. These systems harvest the energy of human motion to power an implant. The available vibration intensity inside the body is usually not very high [7]. Thus, vibrational or kinetic energy harvesters cannot be considered as an appropriate method to power implantable devices.

Wireless power transfer technology is a promising alternative to batteries as well. Although inductive power transfer [8] and mid-range radio frequency (RF) power transmission [9] are capable of providing wireless power to IMDs, acoustic waves have the potential to be employed in wireless transfer systems to safely provide electrical power to an IMD and have several advantages over other powering techniques. These advantages include lower absorption in tissue, shorter wavelength enabling smaller transducers, and higher power intensity threshold for safe operation. Acoustic power transfer systems can provide sufficient power for deeply implanted devices [10]. For a more detailed discussion of different power approaches and in particular acoustic power transfer for implantable medical devices (IMDs) we refer the reader to a recent review [11]. An acoustic power transfer system generally consists of a transmitter outside the human body, and a receiver implanted inside the human body. The transmitter converts the input electrical energy to mechanical energy. The mechanical energy travels through the human body and is captured by the receiver, and is converted to electrical energy to power the IMD.

For an acoustic power transfer system, the power delivered to an IMD in human tissue is dependent on several system parameters: load impedance, operating frequency, receiver position relative to the transmitter, and receiver and transmitter size. As the position and orientation of the implant cannot be perfectly controlled, it is essential to consider the effect of the uncertainty of position and orientation of the implanted receiver on power transfer. Variation in position and orientation can be characterized using three parameters: depth, angle, and offset. Depth is the axial distance between the transmitter and receiver. Angle or orientation is defined as the angle between the receiver face and the transmitter face. Offset or alignment is the lateral distance between the center of the transmitter and center of the receiver. Any change in the location of the receiver may result in a drop in the generated power and may lead to a power level which is not sufficient for the IMD. In some cases, a lateral offset equal to the diameter of the receiver may result in approximately 70% drop in the generated voltage [12]. The drop could also be worse for the generated power as it is a function of voltage squared. The majority of literature in the area of acoustic power transfer for IMDs reported voltage or power delivered to the load as a function of depth or offset [13–15]. There are few researchers that have thoroughly investigated the dependency of power to depth, angle, and offset [16]. The sensitivity of the generated power to any change in the location of the receiver needs to be fully studied. This sensitivity may depend on the operating frequency as operating at lower frequencies which have longer wavelength can result in devices that are less sensitive to offset and alignment mismatches. As there are several types of ultrasonic receivers with different resonance frequencies, it is necessary to study the effect of working in different frequencies on the sensitivity of the generated power to any change in the location of the receiver.

Capacitive micromachined ultrasonic transducers (CMUTs) have also been employed for wirelessly transferring power using a comb drive to generate electrical energy from a base vibration [17, 18]. The small gap required for achieving high sensitivity limits the potential generated acoustic power by reducing the deflection of the plate. CMUTs require large bias voltage which may create safety concerns. They have inherently nonlinear transduction mechanism that may introduce significant circuit design challenges [19]. Piezoelectric transducers are an alternative solution to these problems. Conventional ultrasonic transducers that may be employed for acoustic energy transfer are mostly based on commercial off-the-shelf (COTS) bulk piezoelectric materials, i.e. plate structures, with high acoustic impedance and poor acoustic coupling to human tissue. On the other hand, piezoelectric micromachined ultrasonic transducers (pMUTs), i.e. diaphragm structures, have lower acoustic impedance due to the lower stiffness of the membrane structure. Small element size and easy integration with supporting electronics are other advantages of pMUTs compared to COTS bulk piezoelectric transducers [20]. The thickness of pMUTs is much smaller than the wavelength while the thickness of bulk transducers needs to be half of the wavelength. So, using pMUTs would result in smaller devices compared to bulk structures when operating at the same frequency. Furthermore, for the same size of a receiver, diaphragm structures would have lower resonance frequencies. The bulk piezoelectric structure is widely used in therapeutic and diagnostic applications; however, the pMUT structure seems to be a better candidate for acoustic power transfer for IMDs in which the receivers are very small since this architecture is capable of generating more power than the bulk structure and is significantly less sensitive to changes in implant location for generator diameters in the sub-millimeter range [21]. Christensen and Roundy compared COTS plate and diaphragm mode structures for an acoustic power transmission system and numerically showed that the diaphragm structure is significantly less sensitive to changes in implant offset and angle. Although the pMUT seems to be a better candidate, the number of publications fabricating a microelectromechanical systems (MEMS) receiver are sparse compared to those using COTS transducers. One issue is that there is a significant gap in available piezoelectric material thickness between MEMS and COTS transducers. COTS piezoelectric transducers are typically available in thicknesses higher than 127 μ m (0.005") since this is the thinnest available bulk piezoelectric layer. On the other hand, MEMS piezoelectric processes can only fabricate layer thicknesses up to about 6 μ m. [22]. In this paper, we present a MEMS fabrication process to fabricate pMUT devices with thicknesses in the range of 6 μ m–127 μ m.

The purpose of this paper is to provide a comprehensive comparison between two common piezoelectric ultrasonic transducers for powering implantable devices. To this end, load voltage and power of these structures as a function of depth, orientation, and alignment are fully studied and compared together. Although both of these structures have been studied in the literature separately, there is no such an experimental analysis to compare these two structures. In order to fully explore the comparison of MEMS and COTS ultrasound transducers, we propose a new fabrication process that can bridge the gap in available piezoelectric layer thicknesses. We theoretically and experimentally analyze the performance of the fabricated device in the presence of uncertainties and compare its performance to a COTS device. The analysis provides insight into the conditions in which a MEMS scale diaphragm would be preferred as the receiver over a COTS transducer for a robust acoustic transfer system considering power loss due to disturbances in depth, orientation, and alignment.

2. Frequency selection for an acoustic power transfer system

The acoustic power transfer system needs to operate at a certain frequency. The resonance frequency of the receiving transducer is usually selected as the operating frequency, which results in maximum transferred power. Resonance frequencies are determined by the geometry of transducer and material constants. Generally, there are constraints on the size of the receiver as it needs to be implanted inside the human body. For a given size constraint, different transducers would have different frequency characteristics, which will be discussed in the next section. The operating frequency can affect the performance of the acoustic transfer system since several factors such as tissue attenuation, and Rayleigh distance are strong functions of frequency. To fully understand these effects, we need to first cover some basics of acoustics and beam patterns for an acoustic transmitter in this section. The behavior of this beam pattern is critical in understanding the sensitivity of the generated power to the location of the receiver.

For a circular unfocused bulk thickness-mode transducer, the acoustic beam radius is approximately equal to the radius of the transducer up to a certain distance, but it begins to spread at larger distances. In the region near the transducer (near-field), the pressure magnitude oscillates (i.e. has spatial resonances) resulting in multiple minima and maxima as one moves away from the face of the transmitter. This irregularity in amplitude, which is due to the interference between contributing waves from all parts of the transducer face, makes the power transfer unpredictable. However, in the regions further from the transducer face (far-field), the beam shape is more uniform and decays with increasing distance.

The pressure on the face of the receiver can be derived using Huygens principle. This principle calculates the pressure generated by an ultrasound transducer at any distance from the transducer face. Every point on the transducer face is assumed to be a radiator of a spherical pressure wave and considered as a point source. The pressure at any observation point is the contribution of all spherical waves from all point sources. For a circular transmitter as shown in figure 1 whose face is vibrating with a sinusoidal pressure with magnitude p_0 and angular frequency ω , the total pressure at the observation point is [23]:

$$p = \frac{kp_0}{2\pi} \int_{source} \frac{\cos\left(\omega t - kr' + \pi/2\right)}{r'} \rho d\rho d\theta, \qquad (1)$$

where t is time, r' is the distance from the source points to the observation point, and k is the wavenumber $(2\pi/\lambda)$ assuming λ is the wavelength of the wave. Equation (1) can be solved separately in near-field and far-field. The near-field pattern of a circular transducer with radius a on the z-axis is expressed as [23]:

$$p(z, t) = p_0 \left[\cos(\omega t - kz) - \cos(\omega t - k\sqrt{a^2 + z^2}) \right]. (2)$$

The instantaneous acoustic intensity is the acoustic power per unit area. The acoustic intensity in a medium with the acoustic impedance Z is defined as:

$$I(z, t) = \frac{p^{2}(z, t)}{Z} = \frac{p_{0}^{2}}{Z} \left[\cos(\omega t - kz) - \cos(\omega t - k\sqrt{a^{2} + z^{2}}) \right]^{2}.$$
(3)

Equation (2) only holds for on-axis observation points and gives the on-axis pressure amplitude. The irregular pressure pattern in near-field can be described by this equation. The first term in equation (2) contains the contribution of pressure coming from all points on the face of the transducer. The second term contains the contributions of pressure coming from all points at the perimeter of the transducer and subtracts from the first term. As the distance between the transducer and the observation point increases, the phases of the first and second terms change at different rates resulting in a constructive/destructive interference pattern. The pressure magnitude is plotted in figure 2 for a circular transducer with radius a for a frequency range of 100 kHz-1 MHz. In the near-field, there are some points at which the pressure magnitude is zero resulting in zero output power. The transition between near-field and far-field occurs at a distance called Rayleigh distance. The Rayleigh distance increases with the increase in the operating frequency. Thus, at higher frequency the near-field is longer, so the receiver is more likely to be in the near-field. And when the receiver is in the near-field, there is a constructive/destructive interference pattern along the face of the receiver, so as the receiver moves axially that interference pattern will change and the output power will significantly change. It should be mentioned that operating at higher frequencies would result in higher pressure at a given distance. However, this may come at tradeoff in robustness to misalignment and misorientation.

In far-field, equation (1) can be calculated for any point, not just points along the transmission axis. This is due to the fact that the distance between the transmitter and the observation point is large enough to make some simplifications. The pressure profile and acoustic intensity for a circular transducer at any point (off-axis as well as on-axis) when the beam is observed in the far-field are [23]:

$$p(r,\phi,t) = \frac{\pi a^2 p_0 \sin(\omega t - kr)}{\lambda r} \left[\frac{2J_1(ka \sin \phi)}{ka \sin \phi} \right], \quad (4)$$

$$I(r,\phi,t) = \frac{\pi^2 a^4 p_0^2 \sin^2(\omega t - kr)}{\lambda^2 r^2} \left[\frac{2J_1(ka\sin\phi)}{ka\sin\phi} \right]^2, \quad (5)$$

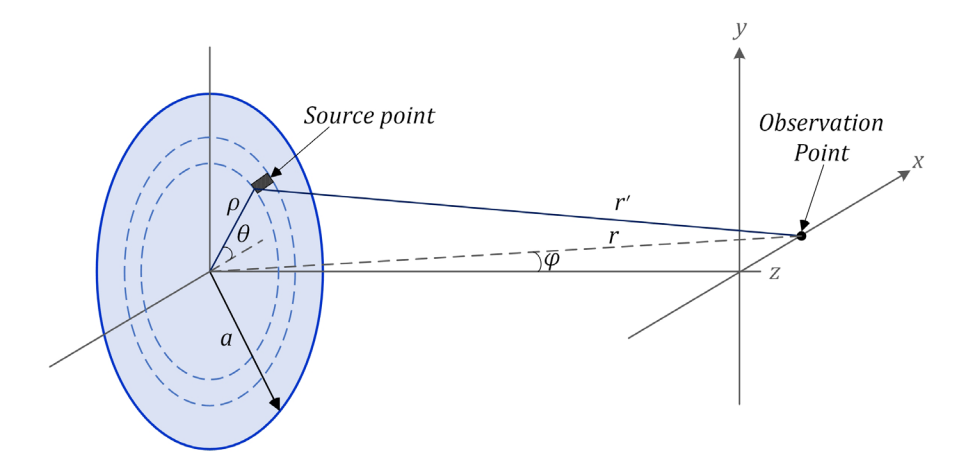


Figure 1. Geometry of a circular transmitter.

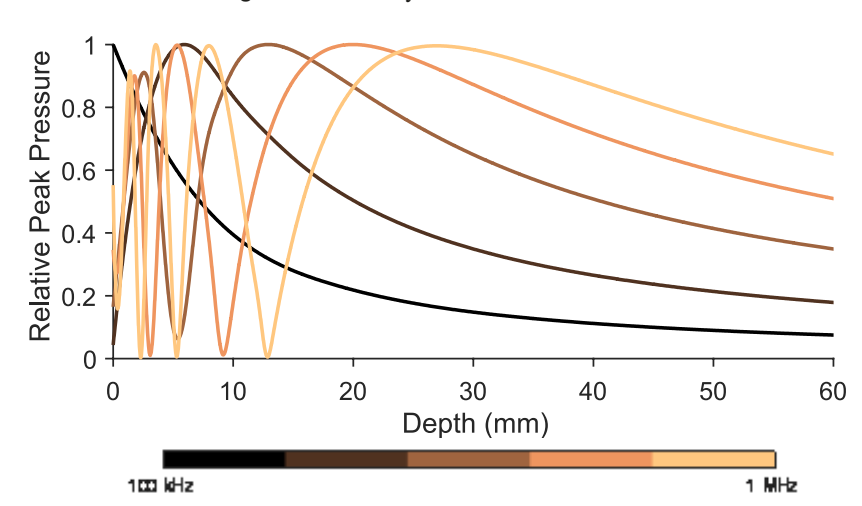


Figure 2. Relative on-axis peak pressure magnitude from a transducer with radius a at one particular time t = 0.

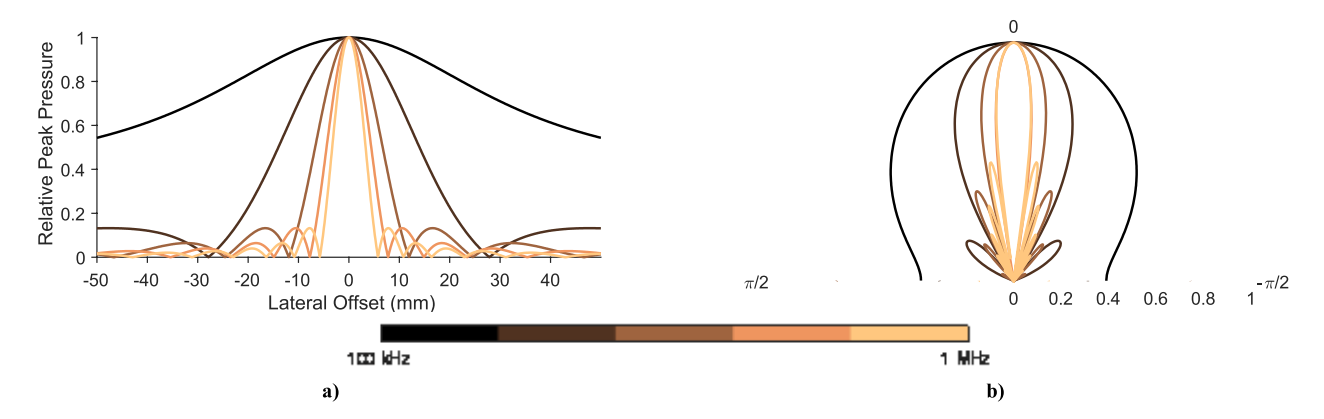


Figure 3. (a) The far-field pressure pattern from a transducer with radius *a* versus lateral offset; (b) an angular plot of the far-field pressure pattern in polar coordinates (the pressure is plotted in decibel units).

where J_1 is the Bessel function of the first kind with order 1. As we expected, the pressure in far-field has an inverse relationship with the distance, r. The term in the square bracket, which is called directional factor, is 1 at on-axis points and starts to decrease as the lateral distance between the transducer and the observing point increases. The normalized acoustic intensity at far-field is plotted against the lateral distance for a circular transducer in figure 3 for a frequency range

of 100 kHz–1 MHz. As shown in figure 3, at higher frequencies the pressure can drop significantly due to small changes in the lateral offset, which makes operation at high frequency very sensitive to any misalignment and misorientation of the receiver. As the receiver rotates or becomes misoriented with regard to the transmitter, a pressure gradient across the surface of the face results in decreasing the average pressure seen by the receiver. Any transducer that operates at high frequencies

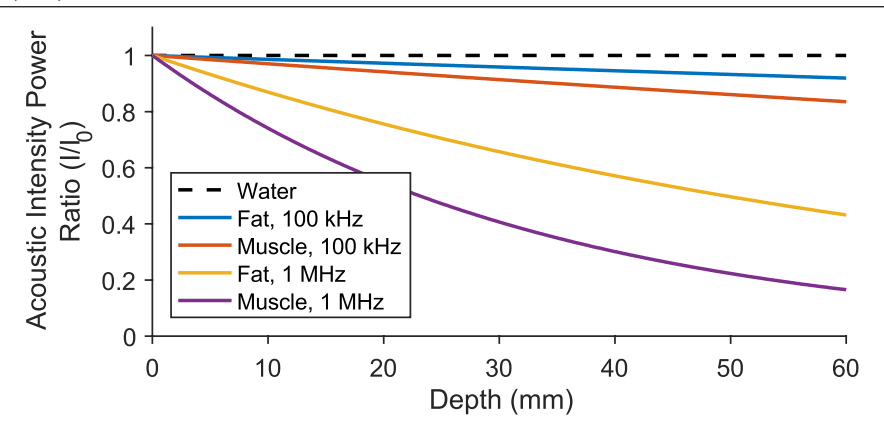


Figure 4. The effect of attenuation for different operating frequencies in different mediums.

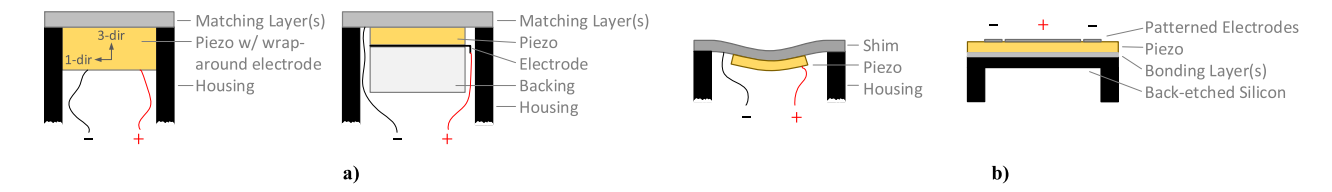


Figure 5. Two common piezoelectric structures for acoustic power transfer, (a) plate structure; (b) diaphragm structure.

will probably have similar sensitivity. Therefore, it is possible to improve the robustness of the ultrasonic receiver by operating it at lower frequencies.

Attenuation in human tissue strongly depends on the operating frequency. Attenuation in acoustics is the drop in the amplitude of the ultrasound beam as a function of distance through the human tissue. As the pressure wave travels through the medium, i.e. the human body, it is absorbed in the tissue. This reduction is expressed as:

$$I(z) = I_0 e^{-2\alpha z},\tag{6}$$

where I_0 is the unattenuated acoustic intensity at the face of the transmitter, and I is the attenuated acoustic intensity at distance z from the transmitter. The attenuation factor α changes with frequency based on $\alpha = \alpha_0 f$ in which f is the frequency in MHz and α_0 is the attenuation factor at 1 MHz. The attenuation factor in water is very low and near zero, however, the attenuation factor for the human body is not. The attenuation factor at 1 MHz for fresh fat and human muscle is $0.07 \, \mathrm{cm}^{-1}$ and $0.15 \, \mathrm{cm}^{-1}$, respectively [24]. Figure 4 shows the ratio of power at a certain distance to the unattenuated power for muscle and fat mediums in two frequencies $100 \, \mathrm{kHz}$, and 1 MHz. It is clear from the figure that at higher frequencies, the attenuation would be a significant problem and it is beneficial to design devices that can operate at lower frequencies.

3. Structures for ultrasonic piezoelectric power receivers

Piezoelectric power transducers are the most common types of ultrasonic receivers to convert acoustic energy into electrical energy. Two common piezoelectric structures suitable for acoustic power transfer are the plate and the diaphragm structures shown in figure 5. A bulk mode plate structure

is a piezoelectric disk operating at 3-3 mode in which the poling axis is in the same direction as the dominant strain (both perpendicular to the face of the plate). To operate at 3–3 mode, the diameter to thickness ratio of the plate needs to be in the range between 1 to 10. The resonance frequency of a plate structure only depends on its material and its thickness. A plate structure for transmitting and receiving power is most commonly used in the literature. For optimal performance, the thickness of the piezoelectric layer should be half the acoustic wavelength in the piezoelectric material. The acoustic wavelength in PZT at 1 MHz is approximately 4 mm. For the piezoelectric element to be much thinner (significantly below 1 mm) and operate efficiently, the frequency must go up. The resonance frequency has an inverse relationship with the thickness, and therefore, small receivers have a higher resonance frequency. At millimeter thicknesses, the resonance frequency is on the order of megahertz resulting in high tissue absorption. The resonance frequency for a PZT material with speed of sound 4080 m s⁻¹ is plotted against the device thickness in figure 6. As discussed in the previous section, operating at high frequencies results in higher attenuation in mediums like the human body and makes devices more sensitive to orientation and alignment. Some researchers are studying the use of piezoelectric devices with an alternative and more compliant geometries as power receivers [22, 25]. This will enable a thinner device to be used efficiently at lower frequencies resulting in increased generated power.

A piezoelectric unimorph diaphragm can be utilized to more efficiently transduce the acoustic wave at very small receiver sizes. Unlike plate structures that use the thickness-mode motion of a plate, diaphragm structures are based on the flexural motion of a thin elastic layer coupled with a thin piezoelectric layer. This structure operates in 3–1 mode in which the poling axis is perpendicular to the face of the

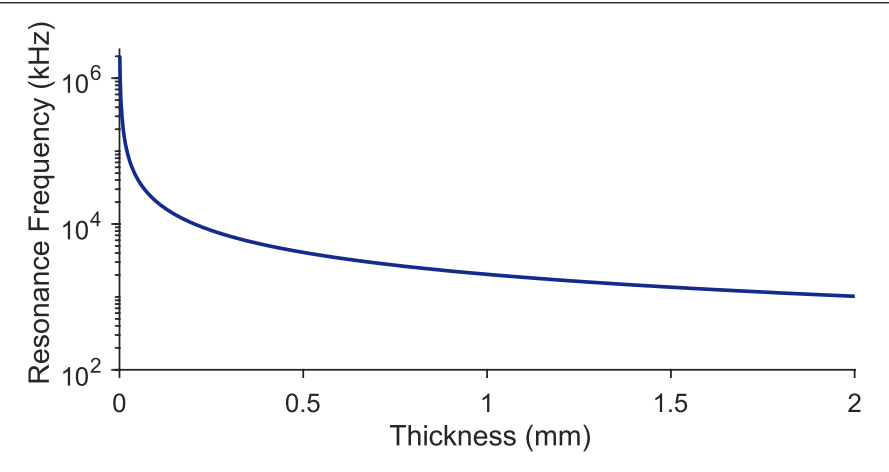


Figure 6. Resonance frequency of plate structures versus the thickness of the plate.

Table 1. Electro-mechanical properties of piezoelectric materials used in pMUTs [32, 34–36].

	Material thickness (μm)	Coupling coefficient, k_{31}^2 (%)	Relative permittivity, ε_{33}	Piezoelectric coefficient, $-d_{31}$ (pm V ⁻¹)
Deposited AlN	<6	3.1-8	8-10.5	1.9–2.3
Deposited PZT	<5	7–25	300-1300	10–100
Bulk PZT	>127	35	1800-3800	190–320

diaphragm (direction 3) whereas the strain is dominant in the direction parallel to the face of the diaphragm (direction 1). In a diaphragm structure, a piezoelectric layer is attached to a non-piezoelectric layer, i.e. shim, to produce a bending mode. This structure has multiple benefits compared to bulk mode plate transducer: its effective acoustic impedance is much lower than that of bulk piezoelectric, its resonance frequency is lower for a given size enabling lower frequency acoustic transmission which has reduced attenuation, and it is more easily achievable in a MEMS format. This diaphragm structure is usually referred to as a piezoelectric micromachined ultrasound transducer or pMUT if implemented as a MEMS device. The resonance frequency of the diaphragm structures is not just a function of its thickness, but depends on the diameter as well. For a similar size, the resonance frequency of a pMUT is typically more than an order of magnitude lower than a plate structure. The resonance frequency, f, for a circular pMUT is [26]:

$$f = \frac{1}{2\pi} \sqrt{\left(\frac{3.2}{a}\right)^4 \frac{D}{\rho}},\tag{7}$$

where a and ρ are the diaphragm radius and area mass density, respectively. D is the flexural rigidity of the structure and is a function of thickness (h), Young's modulus (E) and Poisson's ratio (ν) of all the layers of the diaphragm. For a unimorph diaphragm consisting of an elastic layer and a piezoelectric layer, flexural rigidity is calculated by integrating from the bottom surface of the elastic layer to the top piezoelectric layer:

$$D = \int_{h=0}^{h=h_{Elastic}} \frac{E_{Elastic}h^2}{1 - \nu_{Elastic}^2} dh + \int_{h=h_{Elastic}}^{h=h_{Piezo}} \frac{E_{Piezo}h^2}{1 - \nu_{Piezo}^2} dh.$$
 (8)

According to equations (7) and (8), it is clear that diaphragm devices with smaller thicknesses have lower resonance frequencies that are more suitable for power transfer applications. In other words, at a given operating frequency, diaphragm structures can be smaller compared to plate structures and this makes them more suitable for our specific application of wirelessly powering IMDs. Although these equations are for a circular diaphragm, the dependency of frequency to thickness holds for a rectangular diaphragm as discussed in [27].

The piezoelectric layer of a pMUT is usually achieved by thin film deposition techniques such as sputtering [28], screen printing [29], and sol-gel spin coating [30]. Lead zirconate titanate (PZT) and aluminum nitride (AlN) are two common piezoelectric materials used in pMUTs. The electro-mechanical properties of bulk and deposited PZT, and deposited AlN are summarized in table 1. The maximum achievable thickness for current deposition techniques is about 6 μ m [31]. Growing piezoelectric films thicker than a few microns is particularly challenging because of the large film stress and the tendency to form microcracks [32]. Additionally, as the thickness gets higher than 6 μ m, the piezoelectric layer starts to become more porous. It is true that for two pMUTs with the same piezoelectric material thicknesses (one with PZT and one with AlN), AlN pMUTs show higher optimal receiving sensitivity due to small dielectric constant of AlN and can provide much more voltage; however, PZT can produce higher power from a device. COTS bulk piezoelectric transducers are typically available in thicknesses higher than 127 μ m (0.005"). This leaves a large gap in available piezoelectric material thickness between deposited thin layers and COTS bulk transducers. As discussed in [33], the required thickness for the PZT layer in this study cannot be provided by deposition techniques nor COTS bulk transducers. In other words, in order to have a device with a relatively low resonance frequency around 100 kHz, the total diaphragm thickness around

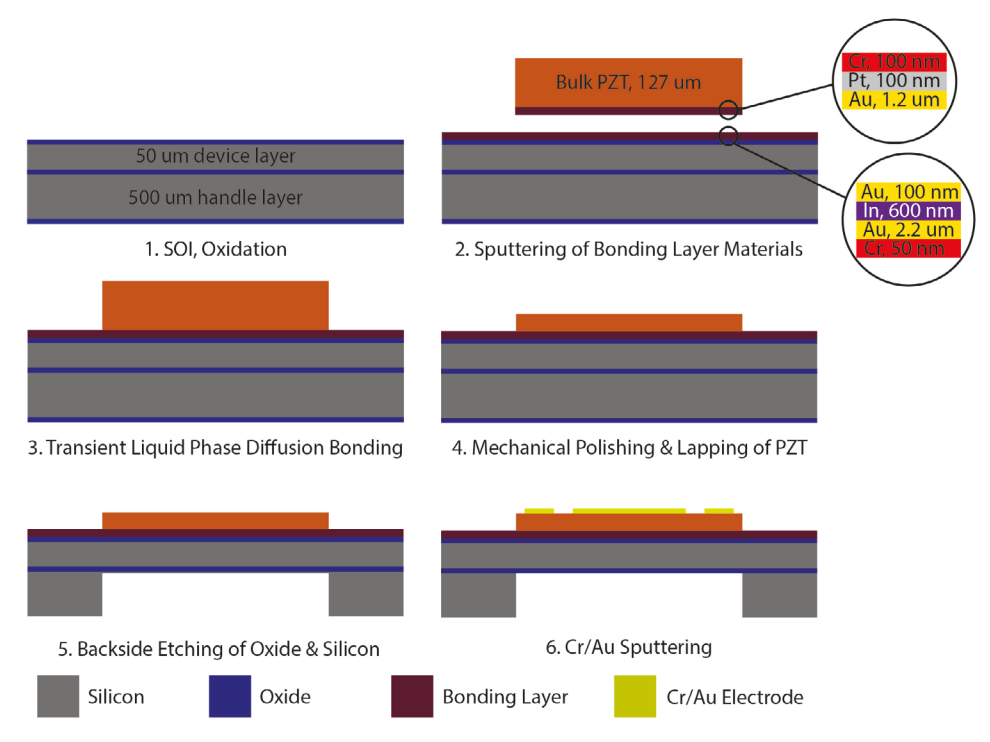


Figure 7. MEMS process flow for very thick PZT devices. The process includes bonding pre-diced pieces of bulk PZT to an SOI wafer to achieve high-quality PZT devices.

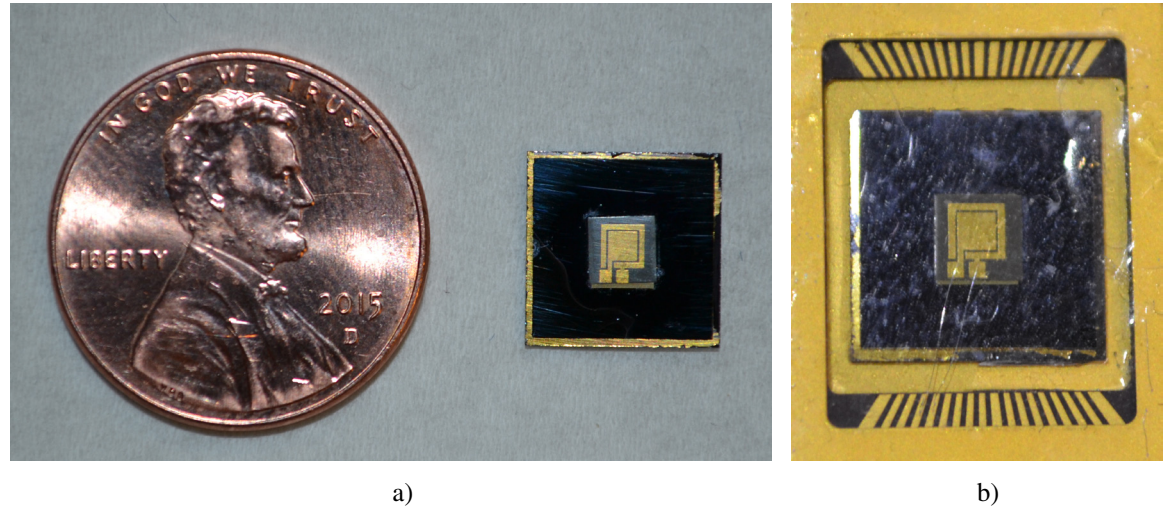


Figure 8. (a) Microfabricated PZT power receiver chip; (b) the packaged microfabricated PZT power receiver.

 $70~\mu m$ is required within a $4~mm^2$ area to get the maximum power. A fabrication process is presented in the following section that uses bulk piezoelectric materials for pMUTs and can bridge the gap in available piezoelectric layer thicknesses.

4. Experimental test setup and model verification

We fabricated a pMUT device using the fabrication process shown in figure 7. The structure is a $2 \, \text{mm} \times 2 \, \text{mm}$ square diaphragm consisting of a piezoelectric layer bonded to silicon. An SOI wafer is used to fabricate the device. First, the bonding layer metals were deposited on the bulk PZT-5A and SOI wafer. Then, the PZT sheet was diced into small square pieces of the desired size. The PZT pieces were then bonded

to the SOI wafer using transient-liquid-phase (TLP) diffusion bonding [37]. In this bonding technique, a low melting point interlayer metal (indium) is sandwiched in between two parent metals (gold). Using this technique, there is no need to repolarize the PZT layer since bonding occurs at low temperatures below the Curie temperature of PZT. It should be noted that the bonding layer is solid to a much higher temperature above the curie temperature after bonding. Mechanical lapping and polishing processes were performed to decrease the thickness of the bulk PZT from 127 μ m to the desired thickness. The diaphragm was created by back-side deep reactive ion etch (DRIE). Finally, the top inner and outer electrodes were patterned by sputtering and lifting off of Cr/Au. Figure 8 shows photographs of the fabricated device. The fabricated pMUT was packaged and then coated with polydimethylsiloxane

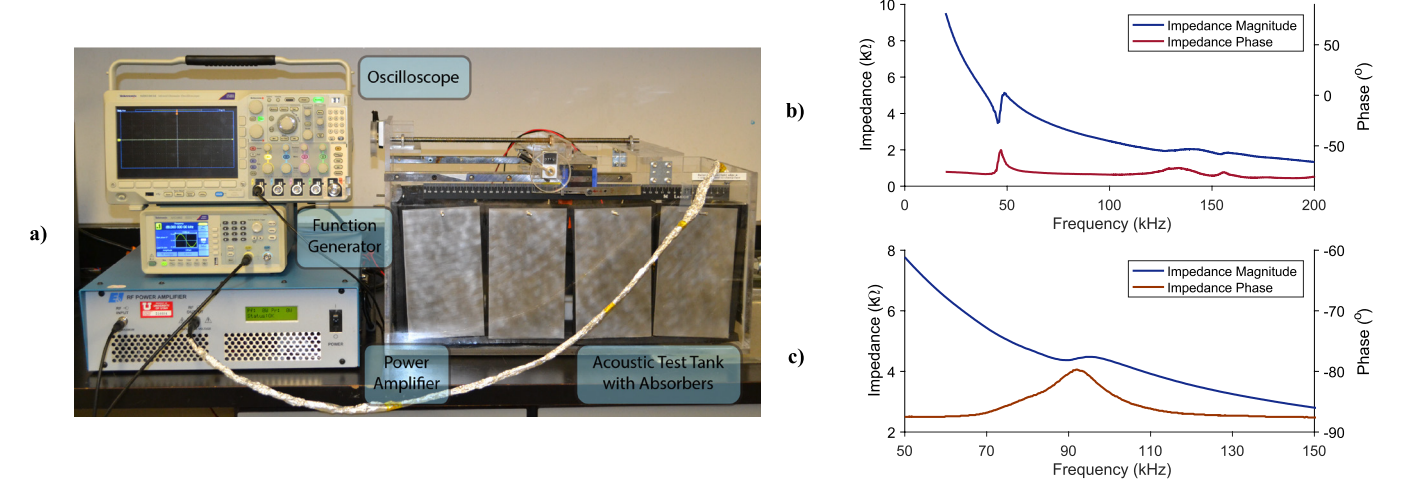


Figure 9. (a) Acoustic test setup for measuring voltage and power; (b) impedance of the bulk transmitter in water; (c) impedance of the fabricated pMUT in water.

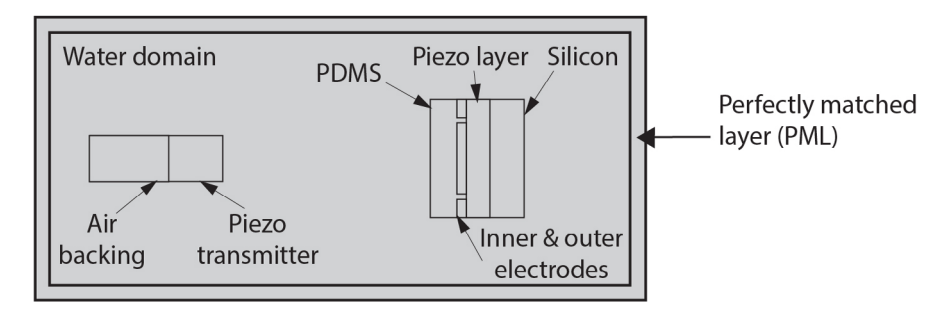


Figure 10. Schematic of the modeled system in COMSOL (top view, not drawn to scale).

(PDMS), which is a bio-compatible silicon-based organic polymer.

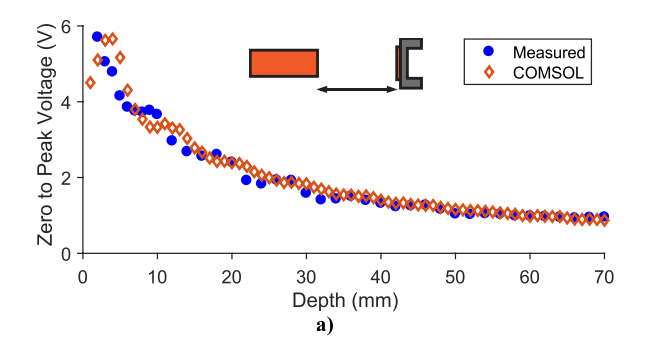
The fabricated pMUT was characterized, and the results can be found in a recently published paper by the authors [33]. The resonance frequency of the pMUT in air and water is 142 kHz and 88 kHz, respectively. The shift in the resonance frequency is due to the added mass effect in which an inertia is added to the system because the device displacement moves some volume of the medium. The performance of the fabricated device in transferring power was investigated in a water-filled acoustic test tank (figure 9(a)) in the presence of depth, orientation and alignment uncertainties. The test tank is a $59 \times 28 \times 28 \,\mathrm{cm}^3$ acrylic tank lined with ultra-soft polyurethane acoustic absorbers. Our test setup enables fine control of the orientation and alignment between acoustic transmitter and receiver. The transmitter is a bulk-mode piezoelectric element that is set atop an ABS tube with cyanoacrylate and sealed against water on the back side. The impedance measurement of the fabricated pMUT receiver and transmitter in water are shown in figures 9(b) and (c). The measurements were performed using an impedance analyzer (Agilent 4294A). The transmitter is powered by a Tektronix AFG1062 function generator connected to an E&I 240L power amplifier. The receiver has an optimal resistive load of $4.3 \,\mathrm{k}\Omega$ connected across its terminals. The optimal load is chosen to be equal to the impedance of the pMUT at 88 kHz. Zero to peak voltage measurements across the receiver load were recorded using a Tektronix MDO3014 oscilloscope, and the generated average

power was calculated using the measured voltage and the receiver load. The input acoustic intensity for all the experiments is set to be 322 mW cm⁻², which is well below the safety limit for ultrasound intensity (720 mW cm⁻²) defined by the United States Food and Drug Administration (FDA) [38]. During the tests, the location of the receiver was changed with respect to the transmitter, and the receiver load voltage was measured and recorded. The power generated (measured and simulated) across the optimal load is plotted versus the depth of the receiver, alignment, and orientation of the receiver in figures 11–13, respectively. The voltage measurements are also provided as a practical reference as most power conditioning schemes will require a minimum voltage to operate.

The COMSOL model used in this study includes the fabricated receiver, transmitter, and the medium as shown in figure 10. Modeling techniques such as circuit equivalent models and 2D axisymmetric finite elements are unable to model the effects of orientation and alignment. While a simplified 1D model can provide a general guide, a three-dimensional (3D) model and simulation are necessary to study the effects of depth, orientation, and alignment for a square diaphragm. First, the pMUT is modeled. The lowest layer of the pMUT is silicon. On top of that, there is the piezoelectric layer made of PZT-5A. Above the piezoelectric layer are the inner and outer Au electrodes creating access to the generated AC potential. The topmost layer of the pMUT is PDMS. Both the inner and outer electrode layers are 0.3 μ m thick and modeled as separate structural layers. The width of the square

Table 2. Properties of the piezoelectric material, silicon, and water medium used in the COMSOL simulations.

	Unit	Piezo Transmitter	pMUT				
			Piezo	Silicon	Gold electrodes	PDMS	Water
Diameter	mm	12.8					
Length	mm		2	2	1.4 (inner electrode)	2	
Thickness	mm	28.65	0.04	0.05	0.0003	0.3	
Density	${\rm kg}~{\rm m}^{-3}$	7600	7800	2330	19300	965	1000
Speed of sound	${ m m~s^{-1}}$	4080	3900	8433	3240	2200	1500
Young's modulus (Y_1^E)	Pa	63×10^{9}	61×10^9	166×10^9	70×10^{9}	2.36×10^{6}	
Young's modulus (Y_3^E)	Pa	54×10^{9}	52×10^{9}				
Poisson's ratio		0.32	0.32	0.27	0.44	0.4	
Charge constant $(-d_{31})$	$\mathrm{pm}\mathrm{V}^{-1}$	175	190				
Relative permittivity	•	1900	1800				



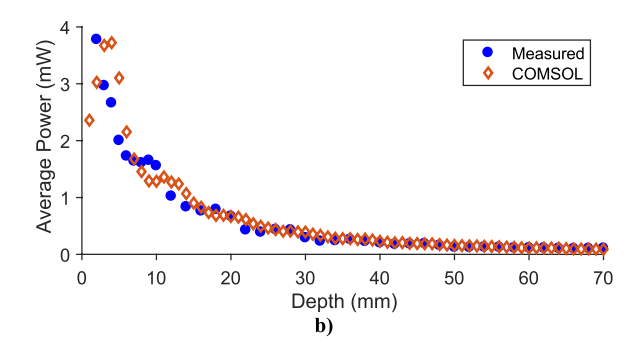


Figure 11. (a) Generated peak voltage and (b) generated average power versus receiver depth at $88 \, \text{kHz}$ at $0 \, \text{mm}$ offset and 0° angle for the fabricated pMUT.

device is 2 mm. The transmitter model consists of a piezoelectric layer and an air backing layer. The transmitter and the receiver are modeled inside a water domain. A perfectly matched layer (PML) is used to model the absorption of sound waves as they propagate far away from the sound source. The PML reduces the effect of any reflection from the edges. The dimensions of all system constituents and the material properties used for the simulations are given in table 2. The acoustic-piezoelectric interaction, frequency domain interface is used to simulate the acoustic power transfer system. The pressure acoustics interface solves the wave equation in the medium. The solid mechanics interface is solved on all structural materials including piezoelectric materials, silicon, and electrodes. Silicon is considered as an anisotropic material. The electrostatics interface is only solved on the piezoelectric material layers. The electrical equat1ions are not solved in the metallic gold layers because the electrical conductivity of gold is many orders of magnitude higher than that of PZT and hence the gold layers act as equipotential regions allowing extremely small conduction current through them. Thus, the electrical characteristics of electrode layers do not have any significant effect on the response of the pMUT. The maximum mesh element size is specified as 1/5th of the wavelength to accurately resolve the pressure waves within the inner water domain. The total number of degrees of freedom solved for is 675873 for COMSOL simulations. The COMSOL finite element simulation used 75 321 elements for the transmitter, 268 989 elements for the pMUT, and 331 563 elements for the medium.

According to figure 11, the trend of simulation and experimental data matches, and this trend indicates that the device is operating in far-field and away from the Rayleigh distance as the power profile is uniformly decreasing with depth. The operating resonance frequency 88 kHz results in a wavelength of 17.04 mm and Rayleigh distance 2 mm in water. Another important takeaway from this graph is that the system is capable of generating about 0.5 mW of average power (1 mW of peak power) in distances between 20 mm to 30 mm. The pMUT device is also capable of producing about 0.23 mW of average power (0.46 mW of peak power) at a depth of 40 mm with zero offset and angle. The generated power decreases when the receiver is moved axially away or laterally from the transducer. For example, as shown in figure 12, when the receiver has a 10 mm lateral offset, the generated power drops by about 36% and the voltage drops by 20%. The plate structure is more sensitive to change in the offset of the receiver and we will investigate this comprehensively in the next section. The results for the angle experiment (figure 13) are only valid in the angle range of -5° to $+5^{\circ}$. This is due to the fact that the package of the pMUT is much larger than the pMUT size. When the device has an angle not in that range, the incoming acoustic wave hits the package and not the device, which can cause the voltage and the power to drop faster than predicted by simulation. In other words, the size of the package is bigger than the size of the device itself, so when we rotate the device, the upcoming pressure wave hits the package first resulting in a faster power drop in experimental data. We did not model the whole package in our COMSOL simulation.

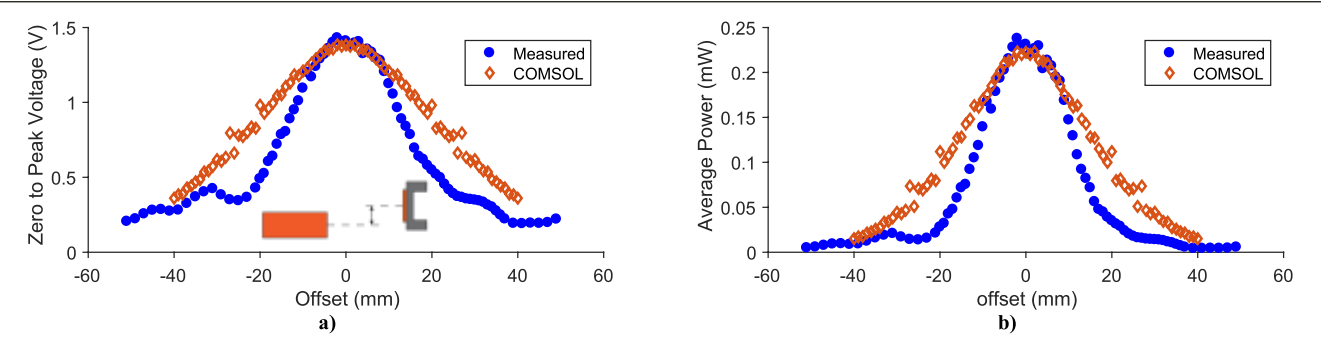


Figure 12. (a) Generated peak voltage and (b) generated average power versus receiver offset at $88\,\mathrm{kHz}$ at $40\,\mathrm{mm}$ depth and 0° angle for the fabricated pMUT.

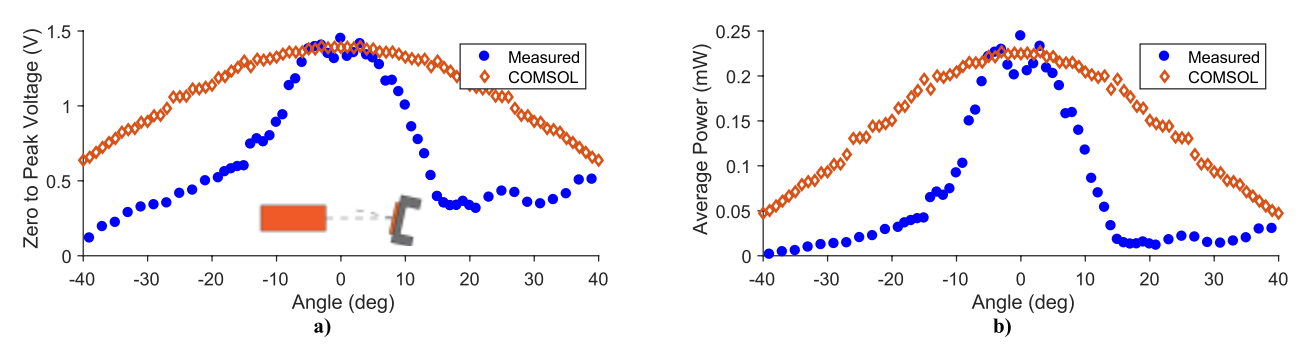


Figure 13. (a) Generated peak voltage and (b) generated average power versus receiver angle at 88 kHz at 0 mm offset and 40 mm depth for the fabricated pMUT.

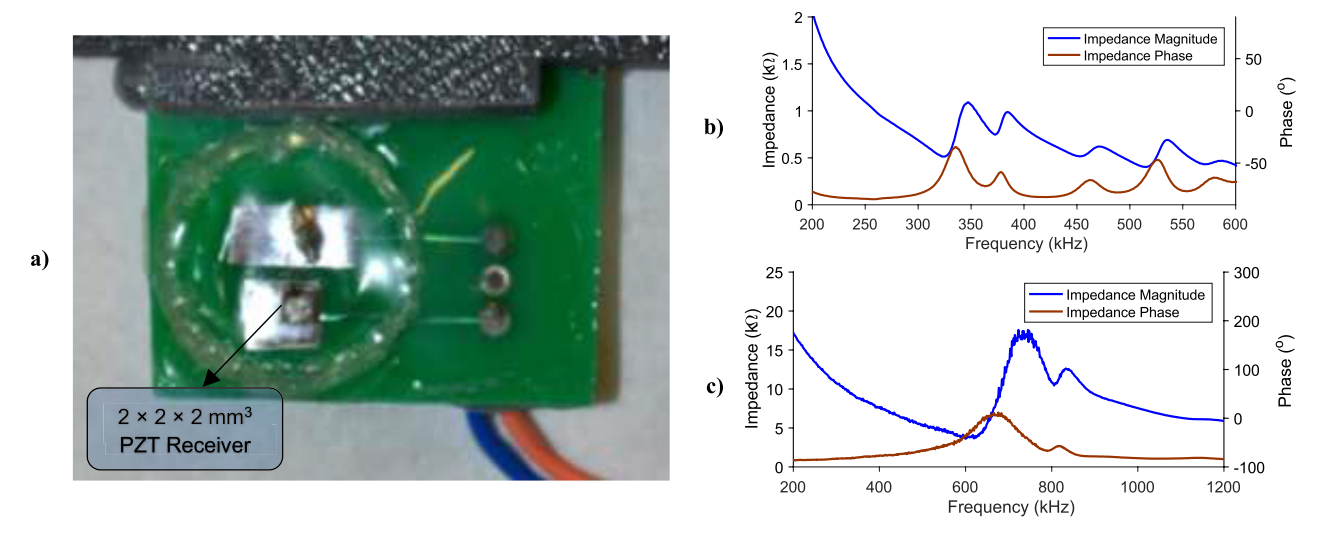


Figure 14. (a) The packaged COTS bulk receiver; (b) impedance of the bulk transmitter in water; (c) impedance of the COTS bulk receiver in water.

5. Generated power and sensitivity comparison

To compare the results of our pMUT to a COTS bulk piezo-electric transducer, we used a bulk PZT with a similar area to the fabricated device. Please note that we did not match the thickness of the COTS transducer to our pMUT since it would result in a very high resonance frequency. The COTS device is a $2 \times 2 \times 2$ mm³ PZT-5A and is attached to a PCB and coated with PDMS as shown in figure 14(a). The COTS bulk receiver was tested in the same acoustic tank. The device was characterized in air and water. The resonance frequency of the device in air and water is 658 kHz and 628 kHz, respectively. The

resonance frequency slightly drops for plate structures as they have smaller displacement compared to diaphragm structures. We chose another transmitter that has a similar resonance frequency to the receiver, which is a bulk-mode piezoelectric element that is set atop an ABS tube with cyanoacrylate and sealed against water on the back side. The piezoelectric element is 12.7 mm in diameter, 3.43 mm thick, and has a standard separate electrode on each face. The impedance results of the bulk receiver and transmitter in water are shown in figures 14(b) and (c). The impedance response of the transmitter shows some lower frequency peaks, which are from the radial vibration mode and harmonics. The impedance of the COTS

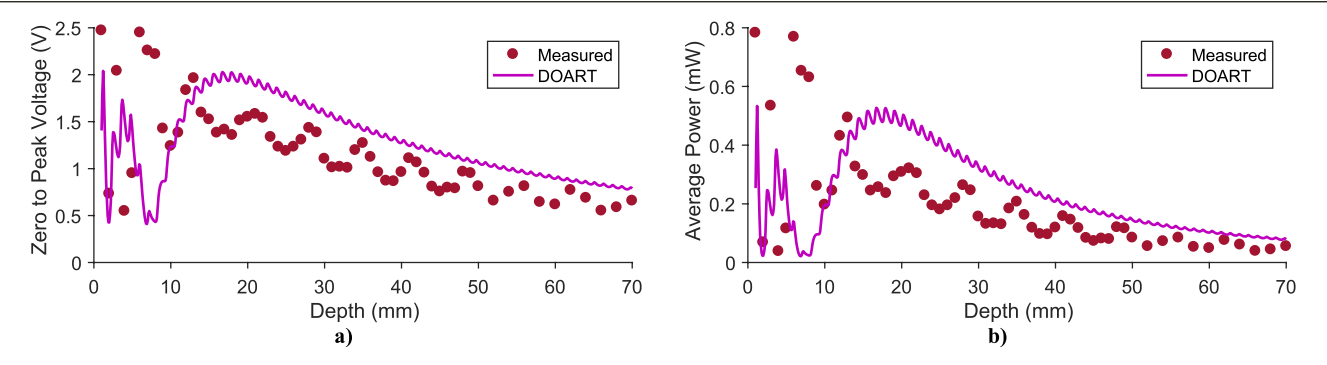


Figure 15. (a) Generated peak voltage and (b) generated average power versus receiver depth at $88\,\mathrm{kHz}$ at $0\,\mathrm{mm}$ offset and 0° angle for the COTS bulk receiver.

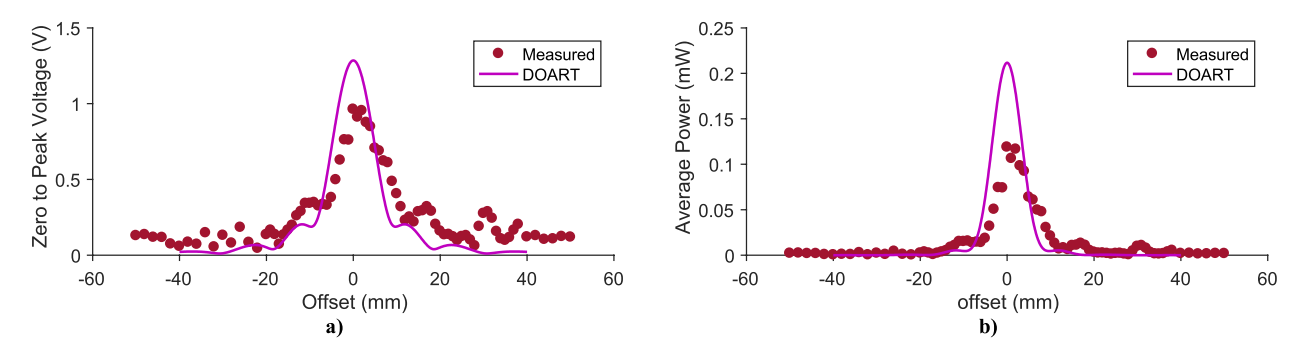


Figure 16. (a) Generated peak voltage and (b) generated average power versus receiver offset at 88 kHz at 40 mm depth and 0° angle for the COTS bulk receiver.

device at its resonance frequency is $3.9\,\mathrm{k}\Omega$. This was chosen as the optimal load of the bulk transducer. We measured the voltage and calculated the power across the optimal load as a function of depth, offset, and angle for the input power of $322~\mathrm{mW~cm^{-2}}$ at $628\,\mathrm{kHz}$.

Although 3D finite element analysis has the capabilities to model the effects of orientation and alignment, the computational cost is very high as the operating frequency of the acoustic power transfer system goes up. As the frequency goes up, the wavelength becomes shorter, and more elements are needed in meshing the geometry. In order to efficiently model the effects of orientation and alignment in high frequencies, we employed a modeling technique that models the effect of depth, orientation, and alignment via ray tracing (DOART) as presented in [39]. This technique uses Huygens principle to discretize the face of the transmitter into spherically radiating pressure sources. It can be utilized to determine the power transferred to the receiver for any position and orientation. DOART provides a reduction in computational cost that enables a more thorough exploration of the design and operational space of acoustic power transfer systems. Therefore, the measured voltage and power of the COTS bulk receiver are plotted against depth, offset and angle in figures 15–17 and compared with DOART. DOART is capable of modeling circular transducers and not rectangular ones. It also considers an air backing layer for the transducers, which is not the case in our COTS receiver. With these considerations, we modeled a circular receiver with the same area size to our rectangular COTS receiver and used DOART. The general overpredicting of DOART in voltage values can be attributed to the fact that air backing will result in a better performance. The trend of measured data is in agreement with DOART data. Depth measurements were taken from 1 mm to 70 mm at 0° angle and 0 mm offset. Irregular voltage patterns occur in the nearfield; however, the voltage profile becomes more uniform from about 17 mm depth. The device is capable of producing about 0.12 mW of average power (0.24 mW of peak power) at a depth of 40 mm with zero offset and angle. The generated voltage and power in far-field fluctuate when the axial distance between the transmitter and receiver changes because of acoustic standing waves reflecting back and forth between the transmitter and receiver. The package is not modeled in DOART, which makes the standing waves not as strong as for the measured data. When the transmitter and receiver are relatively close together, the reflection activity between them increases. In the far-field, there would be zero fluctuation in voltage and power if the receiver were perfectly acoustically matched to the medium. The difference between the measured and simulated voltages particularly in the near-field may be attributed to several factors. There may be an error in setting the zero distance between the transmitter and the receiver in the experiment which results in a shift in the experimental data. Also, the fact that DOART models a circular receiver with air backing instead of a rectangular one may result in a different performance.

The performance of the COTS is compared to the pMUT structure. Figure 18 shows the measured average power and voltage versus depth for the pMUT and COTS device over the 20–60 mm depth range when angle and offset are equal to zero. This is the range in which both receivers operate at far-field. The results show that voltage and power generally decrease when the depth increases due to beam divergence

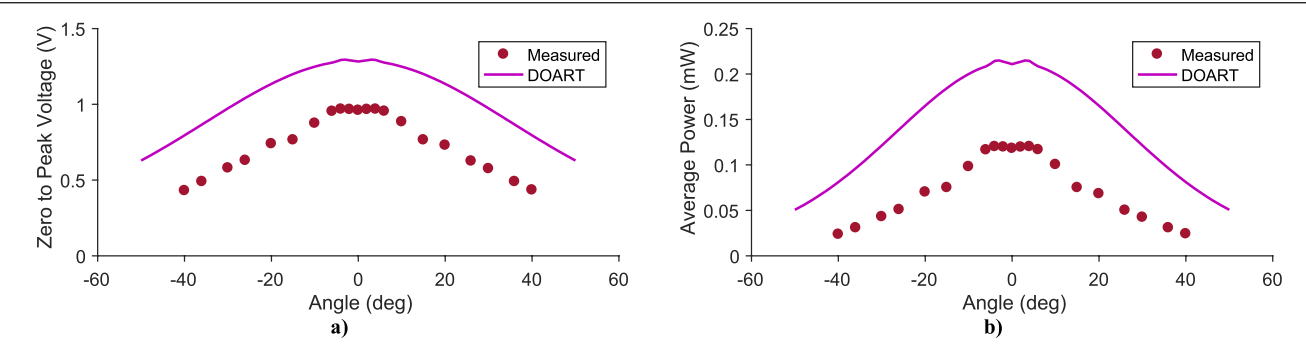


Figure 17. (a) Generated peak voltage and (b) generated average power versus receiver angle at 88 kHz at 0 mm offset and 40 mm depth for the COTS bulk receiver.

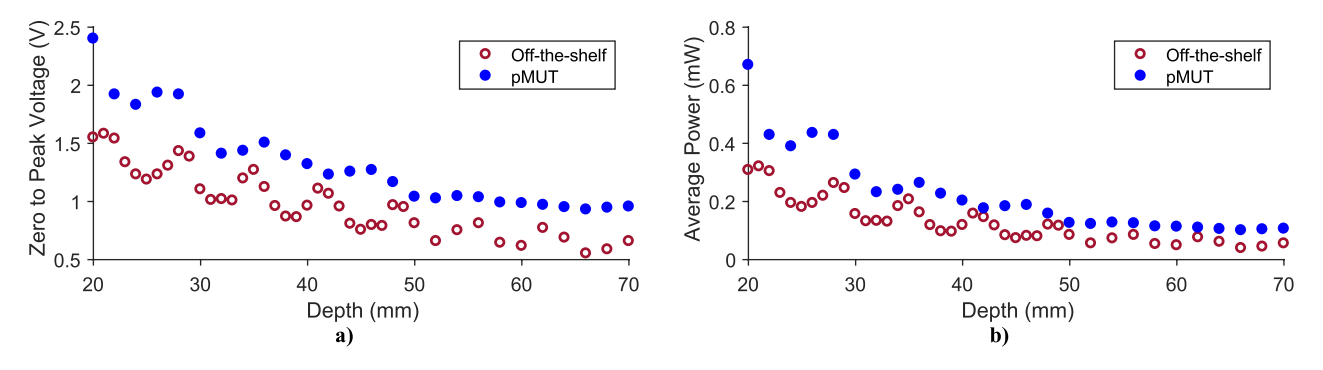


Figure 18. (a) Generated peak voltage and (b) generated average power versus receiver depth at 0 mm offset and 0° angle for the pMUT device and COTS bulk receiver.

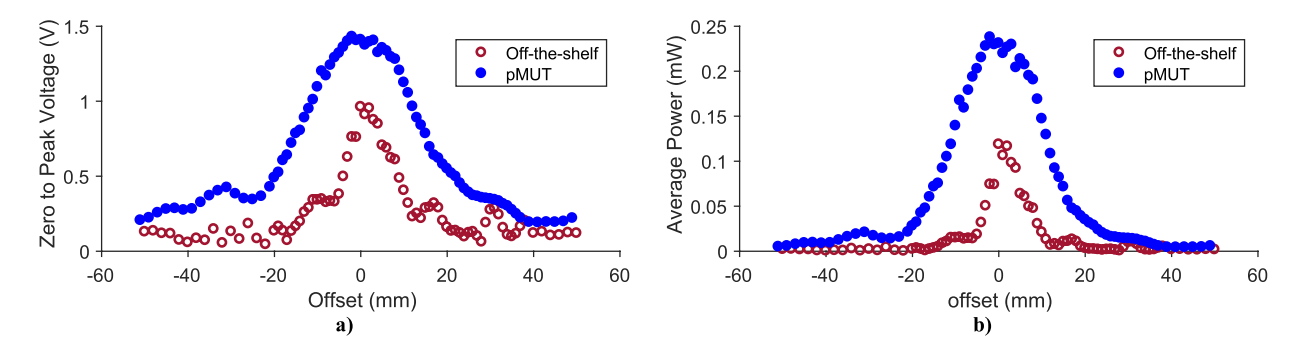


Figure 19. (a) Generated peak voltage and (b) generated average power versus receiver offset at $40 \,\mathrm{mm}$ depth and 0° angle for pMUT device and COTS bulk receiver.

and absorption. Although the COTS device is less sensitive to change in the depth in shallow depths, it has a similar sensitivity to the pMUT as the depth increases. Please note that these results are in a water medium, which has a very low attenuation. In the real applications in the human tissue, the sensitivity to depth of a plate structure would increase more than a diaphragm structure due to operating at higher frequencies as discussed in section 2 of this paper. The diaphragm structure has a lower acoustic impedance compared to a plate structure. This results in lower reflection from the face of the pMUT and better performance since its acoustic impedance is closer to water. The pMUT seems to generate slightly more voltage and power at any depth compared to the COTS device. This is in agreement with the numerical results published in [21] in which a diaphragm structure at about 4 mm² size scale would generate slightly higher power numbers compared to a plate structure with the same size at depths higher than 20 mm when a same acoustic input is applied.

The measured voltage and power versus offset for the pMUT and COTS devices are shown in figure 19. These measurements were conducted at 40 mm depth and zero angle. This depth was chosen as it is far away from Rayleigh distances of both receivers and it is also in an acceptable depth range for implants. As the offset between the transmitter and receiver increases, the receiver captures less of the transmitted power. The pMUT is operating at 88 kHz, and the COTS device is operating at 628 kHz. Disturbances in the generated voltage and power are a strong function of frequency since higher frequencies result in a narrower beam as discussed in section 2. Therefore, the generated voltage and power of a diaphragm structure are less sensitive to the changes in offset of the implants as expected. When the transmitter and receiver become misoriented, the pressure profile on the face of the receiver changes resulting in smaller average pressure on its face. Figure 20 shows the generated voltage and power of pMUT and COTS device versus angle. As the pMUT

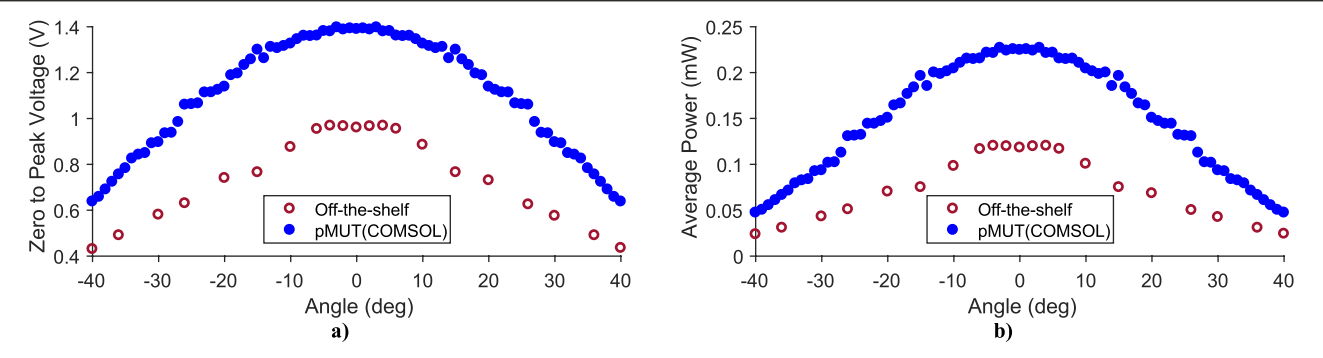


Figure 20. (a) Generated peak voltage and (b) generated average power versus receiver angle at 0 mm offset and 40 mm depth for pMUT device and COTS bulk receiver.

Table 3. Comparison between the performance of our fabricated pMUT and a COTS receiver.

	pMUT Structure	COTS Structure	
PZT size	$2\mathrm{mm} \times 2\mathrm{mm} \times 40~\mu\mathrm{m}$	$2\mathrm{mm} \times 2\mathrm{mm} \times 2\mathrm{mm}$	
Resonance frequency	88 kHz	628 kHz	
Optimal load	$4.3~\mathrm{k}\Omega$	$3.9~\mathrm{k}\Omega$	
Peak input electrical power	417.7 mW (322 mW cm ⁻²)	417.7 mW (322 mW cm ⁻²)	
Output voltage at 40 mm depth, 0 mm offset and 0° angle	1.41 V	0.96 V	
Average output power at 40 mm depth, 0 mm offset and 0° angle	0.23 mW	0.12 mW	
Half power offset	11 mm	3 mm	
Half power angle	27°	20°	
Efficiency at 40 mm depth, 0 mm offset and 0° angle	0.11%	0.057%	
Efficiency at 20 mm depth, 0 mm offset and 0° angle	0.32%	0.15%	
Area normalized efficiency at 40 mm	3.54%	1.83%	
Area normalized efficiency at 20 mm	10.29%	4.82%	

measured data for the angle is not valid at large angles due to the way we packaged the device, we used COMSOL data for the angle comparison. Note that the way we package the COTS device does not affect its angle performance since the incoming acoustic wave can still hit the edges of the misoriented device.

6. Discussion

To quantify the comparison between the pMUT and COTS devices, we defined average percentage improvements in power for all the considered depths, offsets and angles as the ratio of difference in generated power from pMUT and COTS over the generated power of COTS. The average percentage improvement in power are 86%, 917%, and 111% for figures 18–20, respectively. These percentage improvements are the average improvement over all data points shown in figures 18–20. However, as is visually evident, the percentage improvement near zero offset or angle is much lower. At zero offset, for example, the percentage improvement in power is 94%. As the offset increases, the power from pMUT and COTS devices both drop; however, power from COTS device drops much faster. Therefore, at large offsets there are big differences in power numbers between pMUT and COTS devices even when power numbers are relatively very low. The percentage improvement in power for offsets of -5, -10, -20, and -30 mm are 994%, 831%, 1087%, 847%, respectively. This shows the pMUT is capable of providing better power compared to the COTS device. To better compare the performance of two receivers, we also defined a half power offset and angle for the pMUT and COTS devices as the offsets and angles at which power drops by 50%. The comparison results are summarized in table 3.

The output power from both structures is high enough to power an IMD. The power required for IMDs is generally on the order of hundreds of microwatts to tens of milliwatts at the extreme high end [2, 3]. The voltages are also large enough for rectification purposes. The efficiency of the acoustic power transfer system, which is defined by the ratio of generated output power to the input power, may seem low; however, it is higher than the efficiency of similarly sized RF power transmission systems [2]. Furthermore, the efficiency can be improved by addressing two main sources of loss in the current setup. First, the diameter of the transmitter is larger than the receiver, and much of the acoustic energy transmitted is not captured by the receiver. This can be explained by calculating the area normalized efficiency in table 3 as defined in [11]. The area normalized efficiency (the ratio of output power intensity to input power intensity) is a useful metric when the transmitter is large, and the receiver is small. Second, the reflection between the face of the transmitter and water due to acoustic impedance mismatch significantly reduces efficiency. The generated output power can be improved by applying input power intensity closer to the FDA limit and also using matching layers for the transmitter to reduce the reflection between the transmitter and the medium, which were not the focus of this paper. Regarding sensitivity to the location of the

receiver, the half power angle and half power offset are larger for the fabricated pMUT compared to the COTS device. As the size of the receiver decreases, the sensitivity will become more of a major issue for the plate structure as power degrades significantly with implant location because its resonance frequency is very high.

7. Conclusion

In this paper, we presented a MEMS ultrasonic power receiver for powering IMDs, and studied the effect of depth, angle, and offset on the generated power. We developed a 3D COMSOL model and compared the results to the measured data. There is acceptable agreement between the COMSOL simulation and experimental results. The pMUT device is less sensitive to location uncertainties compared to a COTS plate mode transducer with a size similar to the fabricated pMUT. Future work includes addressing the performance of the pMUT device in a full system where the received power can be used to power a bio-medical implant. The fabricated pMUT shows great potential for powering IMDs as it can generate sufficient power (0.23 mW) at large depths. (i.e. 40 mm) and is less sensitive to misorientation and misalignment between transmitter and receiver.

Acknowledgment

The authors gratefully acknowledge funding for this work from the National Science Foundation under Award Number ECCS 1408265.

ORCID iDs

Hamid Basaeri https://orcid.org/0000-0002-7657-2916

References

- [1] Wei X and Liu J 2008 Power sources and electrical recharging strategies for implantable medical devices *Frontiers Energy Power Eng. China* 2 1–13
- [2] Ho J S *et al* 2014 Wireless power transfer to deep-tissue microimplants *Proc. Natl Acad. Sci. USA* 111 201403002
- [3] Eshaghian-Wilner M M (ed)2016 Wireless Computing in Medicine: from Nano to Cloud with Ethical and Legal Implications (New York: Wiley)
- [4] Ben Amar A, Kouki A B and Cao H 2015 Power approaches for implantable medical devices Sensors 15 28889–914
- [5] Karami M and Inman D 2012 Powering pacemakers from heartbeat vibrations using linear and nonlinear energy harvesters Appl. Phys. Lett. 100 042901
- [6] Ansari M and Karami M 2016 Modeling and experimental verification of a fan-folded vibration energy harvester for leadless pacemakers J. Appl. Phys. 119 094506
- [7] Roundy S and Wright P 2004 A piezoelectric vibration based generator for wireless electronics Smart Mater. Struct.
 13 1131
- [8] Silay K, Dehollain C and Declercq M 2011 Inductive power link for a wireless cortical implant with two-body packaging *IEEE Sens. J.* 11 2825–33

- [9] Lu X, Wang P and Niyato D 2015 Wireless networks with RF energy harvesting: a contemporary survey *IEEE Commun.* Surv. Tutorials 17 757–89
- [10] Basaeri H and Roundy S 2017 A micromachined ultrasonic power receiver for biomedical implants *Proc. SPIE* 10164 1016416
- [11] Basaeri H, Christensen D B and Roundy S 2016 A review of acoustic power transfer for bio-medical implants Smart Mater. Struct. 25 123001
- [12] Basaeri H, Christensen D, Yu Y, Nguyen T, Tathireddy P and Young D J 2016 Ultrasonically powered hydrogel-based wireless implantable glucose sensor 2016 IEEE Sensors Proc. pp 1–3
- [13] Meng M and Kiani M 2017 Design and optimization of ultrasonic wireless power transmission links for millimetersized biomedical implants *IEEE Trans. Biomed. Circuits* Syst. 11 98–107
- [14] Shmilovitz D, Ozeri S, Wang C-C and Spivak B 2014 Noninvasive control of the power transferred to an implanted device by an ultrasonic transcutaneous energy transfer link *IEEE Trans. Biomed. Eng.* 61 995–1004
- [15] Shi Q, Wang T and Lee C 2016 MEMS based broadband piezoelectric ultrasonic energy harvester (PUEH) for enabling self-powered implantable biomedical devices Sci. Rep. 6 24946
- [16] Seo D et al 2016 Wireless recording in the peripheral nervous system with ultrasonic neural dust neuron neuroresource wireless recording in the peripheral nervous system with ultrasonic neural dust Neuron 91 1–11
- [17] Fowler A G and Moheimani S O R 2016 4-DOF SOI-MEMS ultrasonic energy harvester *IEEE-NANO 2015—15th Int.* Conf. Nanotechnology pp 1481–4
- [18] Banerji S, Goh W L, Cheong J H and Je M 2013 CMUT ultrasonic power link front-end for wireless power transfer deep in body 2013 IEEE MTT-S Int. Microwave Workshpo Series RF Wireless Technologies Biomedical Healthcare Applications, IMWS-BIO 2013—Proc. pp 1–3
- [19] Smyth K M 2017 Piezoelectric micro-machined ultrasonic transducers for medical imaging Massachusetts Institute of Technology
- [20] Wang Z, Zhu W, Tan O K, Chao C, Zhu H and Miao J 2005 Ultrasound radiating performances of piezoelectric micromachined ultrasonic transmitter *Appl. Phys. Lett.* 86 1–3
- [21] Christensen D B and Roundy S 2016 Ultrasonically powered piezoelectric generators for bio-implantable sensors: plate versus diaphragm J. Intell. Mater. Syst. Struct. 27 1092–105
- [22] Shi Q, Wang T, Kobayashi T and Lee C 2016 Investigation of geometric design in piezoelectric microelectromechanical systems diaphragms for ultrasonic energy harvesting Appl. Phys. Lett. 108 106–11
- [23] Christensen D 1988 *Ultrasonic Bioinstrumentation* (New York: Wiley)
- [24] Goss S A, Johnston R L and Dunn F 1980 Compilation of empirical ultrasonic properties of mammalian tissues. II J. Acoust. Soc. Am. 68 93–108
- [25] Wang T, Kobayashi T and Lee C 2015 Micromachined piezoelectric ultrasonic transducer with ultra-wide frequency bandwidth Appl. Phys. Lett. 106 013501
- [26] Lu Y and Horsley D A 2015 Modeling, fabrication, and characterization of piezoelectric micromachined ultrasonic transducer arrays based on cavity SOI wafers *J. Microelectromech. Syst.* 24 1142–9
- [27] Choi H S, Anderson M J, Ding J L and Bandyopadhyay A 2010 A two-dimensional electromechanical composite plate model for piezoelectric micromachined ultrasonic transducers (pMUTs) J. Micromech. Microeng. 20 015013
- [28] Mehdizadeh E and Piazza G 2018 Through-package wireless powering via piezoelectric micromachined

- ultrasonic transducers *Proc. IEEE Int. Conf. Micro Electro Mechanical Systems (January)* pp 1076–9
- [29] Hindrichsen C G, Lou-Moller R, Hansen K and Thomsen E V 2010 Advantages of PZT thick film for MEMS sensors Sensors Actuators A 163 9–14
- [30] Pardo L J, Jiménez R, García A, Brebøl K, Leighton G and Huang Z 2010 Impedance measurements for determination of elastic and piezoelectric coefficients of films Adv. Appl. Ceram. 109 156–61
- [31] Cassella C and Piazza G 2015 AlN two-dimensional-mode resonators for ultra-high frequency applications *IEEE Electron Device Lett.* **36** 1192–4
- [32] Fu Y Q et al 2017 Advances in piezoelectric thin films for acoustic biosensors, acoustofluidics and lab-on-chip applications Prog. Mater. Sci. 89 31–91
- [33] Basaeri H, Yu Y, Young D and Roundy S 2019 A MEMS-scale ultrasonic power receiver for biomedical implants *IEEE* Sens. Lett. 3 2501104

- [34] Trolier-Mckinstry S and Muralt P 2004 Thin film piezoelectrics for MEMS *J. Electroceram.* 12 7–17
- [35] Khan A, Abas Z, Kim H S and Oh I 2016 Piezoelectric thin films: an integrated review of transducers and energy harvesting Smart Mater. Struct. 25 053002
- [36] Piezo Systems 2019 PSI-5A4E piezoceramic sheets and their properties, piezo systems, Inc (https://support.piezo.com/article/62-material-properties)
- [37] Aktakka E E, Peterson R L and Najafi K 2013 Wafer-level integration of high-quality bulk piezoelectric ceramics on silicon *IEEE Trans. Electron Devices* **60** 2022–30
- [38] FDA 2008 Guidance for industry and FDA staff information for manufacturers seeking marketing clearance of diagnostic ultrasound systems and transducers
- [39] Christensen D B, Basaeri H and Roundy S 2017 A computationally efficient technique to model depth, orientation and alignment via ray tracing in acoustic power transfer systems Smart Mater. Struct. 2006 125020